

# Elastic encapsulation in bicomponent stratified flow of viscoelastic fluids

Pengtao Yue

*Department of Chemical and Biological Engineering and Department of Mathematics, University of British Columbia, Vancouver, BC V6T 1Z3, Canada*

Chunfeng Zhou

*Department of Chemical and Biological Engineering, University of British Columbia, Vancouver, BC V6T 1Z3, Canada*

Joseph Dooley

*The Dow Chemical Company, 433 Building, Midland, Michigan 48667*

James J. Feng<sup>a)</sup>

*Department of Chemical and Biological Engineering and Department of Mathematics, University of British Columbia, Vancouver, BC V6T 1Z3, Canada*

(Received 22 November 2007; final revision received 27 March 2008)

## Synopsis

The second normal stress difference  $N_2$  experienced by non-Newtonian fluids flowing in a pipe may give rise to secondary flows in the transverse direction. As a result, one component tends to encapsulate the other in stratified flows. In multilayer coextrusion, such secondary flows tend to distort the interface and affect layer uniformity. This paper presents numerical simulations of the elastically driven encapsulation in two-component stratified viscoelastic fluids. The simulations are based on a phase-field theoretical model and use finite elements with adaptive meshing to resolve the moving interfaces. The results suggest two mechanisms for elastic encapsulation: One due to the mismatch of  $N_2$  between the components and the other due to noncircular geometry of the cross section. In circular pipes, the more elastic fluid tends to protrude into the other component in the center of the pipe and become encapsulated. This produces the curtate cycloid interface shape commonly seen in experiments. If the cross section is noncircular, both the geometric effect and the elastic stratification are at work, and the interfacial motion is determined by the competition of these two mechanisms. This understanding provides an explanation for the anomalous encapsulation of the less elastic component by the more elastic one observed in multilayer coextrusion. © 2008 The Society of Rheology. [DOI: 10.1122/1.2933436]

## I. INTRODUCTION

Polymer coextrusion is a key process in manufacturing commercial products such as bicomponent fiber, multilayer flat film, and sandwiched foam composites [Han (1981)].

---

<sup>a)</sup>Author to whom correspondence should be addressed; electronic mail: jfeng@chml.ubc.ca

The quality of these products is determined, to a large extent, by the uniformity of the layer structure and the interfacial morphology. Viscosity and elasticity stratification are known to cause interfacial instabilities that develop in the primary flow direction, and these have received much experimental and theoretical investigation [Wilson and Khomami (1993); Khomami and Ranjbaran (1997); Khomami and Su (2000)]. The encapsulation phenomenon, on the other hand, involves distortion of the interface in the plane orthogonal to the primary flow, i.e., the cross section. It is much less studied and is the topic of this paper.

A major factor in the encapsulation phenomenon has been identified as the viscosity difference between the two continuous phases. In *viscous encapsulation*, the less viscous component migrates to the wall and encloses the more viscous component in pipe flows [Lee and White (1974); Southern and Ballman (1975)]. The viscosity contrast determines both the direction and the degree of encapsulation [Lee and White (1974)]. This phenomenon came to be widely recognized from the transport of highly viscous heavy crude oil in pipelines, where the addition of a small amount of water to the crude oil considerably reduces the pressure gradient necessary to drive the flow [Joseph (1997)]. A “minimum viscous dissipation principle” has been invoked to explain the interface shape found in experiment [MacLean (1973); Everage (1973)], although such a variational principle is not rigorously justifiable for flows with interfaces, and is known to fail under certain conditions [Joseph and Renardy (1993)]. Everage (1975) carried out both experimental and theoretical studies on the transient interface motion in a bicomponent tube flow of a nylon/nylon system, and identified two stages in viscous encapsulation. The first stage is characterized by a rapid interface shift caused by the equilibration of the component pressures, and ends within  $2D$  ( $D$  being the tube diameter) downstream the merging point of the two components. The second stage involves the gradual movement of the interface around the tube perimeter, which proceeds downstream for about  $120D$  until complete encapsulation is achieved. The mechanism in the second stage is not yet well understood, but contact line motion definitely plays an important role [Torres *et al.* (1993)].

Another factor, specific to non-Newtonian fluids, is the elastic normal stresses. When non-Newtonian fluids are sheared in a pipe flow, the second normal stress difference  $N_2$  amounts to a lateral forcing in the plane of the cross section. This may cause interfacial motion through two mechanisms. First, if the cross section is noncircular, secondary flows will arise even within a single-component homogeneous fluid. This is a well-known effect and a summary of the literature can be found in Yue *et al.* (2008). This geometric effect will distort the interface between two polymers regardless of their rheological differences [Dooley *et al.* (1998)]. Second, “elastic stratification” in terms of differing  $N_2$  between the components will produce an imbalance of force and thus interfacial deformation even in a circular pipe. White *et al.* (1972), through a simple theoretical analysis, showed that the component with a higher  $-\Psi_2$  tends to protrude into the other one, and eventually be encapsulated. Note that the second normal stress coefficient  $\Psi_2 = N_2 / \dot{\gamma}^2$ ,  $\dot{\gamma}$  being the shear rate, is generally negative. In bicomponent coextrusion through noncircular dies [Khomami and Ranjbaran (1997); Dooley (2002); Dooley and Rudolph (2003)], both mechanisms are at work. For brevity, we will use the term *elastic encapsulation* to refer to interfacial motion driven by elastic normal stresses, even though the secondary flow in noncircular channels usually does not lead to complete encirclement of one component by the other [Dooley *et al.* (1998)].

An interesting question is the interplay between viscosity stratification and elasticity stratification. Coextrusion experiments using polymer pairs suggest the viscosity contrast as the more dominant factor [Lee and White (1974); Khan and Han (1976); Dooley and Rudolph (2003)]. Analysis and computational results have also been used to argue that

elasticity has minimal effects on interfacial motion [White and Lee (1975); Sunwoo *et al.* (2001, 2002)]. Thus elastic effects have been mostly neglected. But some key observations cannot be explained by viscous effects alone. One such phenomenon is the *curtate cycloid* interface shape [Han (1973); Lee and White (1974); Minagawa and White (1975); Southern and Ballman (1975)]; see Fig. 3 of Southern and Ballman (1975) or Fig. 6(a) of this paper. Coextruding two polystyrene melts through a circular pipe at temperature  $T=240\text{ }^{\circ}\text{C}$ , Southern and Ballman (1975) attributed this extraordinary interface shape to a viscosity crossover, i.e.,  $\mu_A > \mu_B$  if  $\dot{\gamma} > \dot{\gamma}_c$  and  $\mu_A < \mu_B$  if  $\dot{\gamma} < \dot{\gamma}_c$ , where  $\mu$  is the shear viscosity,  $\dot{\gamma}_c$  is the shear rate at the crossover, and A and B denote the two components. Thus when the average shear rate in the pipe is around  $\dot{\gamma}_c$ , component A is less viscous than B at the tube center where  $\dot{\gamma}$  is low, but more viscous near the wall where  $\dot{\gamma}$  is high. They argued that this would lead to opposite interfacial motion in the two regions and hence the curtate cycloid shape. However, when the same experiment was repeated at  $T=220\text{ }^{\circ}\text{C}$ , at an average shear rate around the now lower  $\dot{\gamma}_c$ , the curtate cycloid shape failed to appear. Furthermore, Karagiannis *et al.* (1990) and Torres *et al.* (1993) simulated Southern and Ballman's experiments by matching their shear viscosity data using an inelastic Carreau model. Again, no curtate cycloid shape was predicted by the three-dimensional (3D) numerical calculations. These cast doubts on the explanation based on a viscosity crossover. Could melt elasticity be the real cause of the curtate cycloid shape?

Another notable phenomenon is the *anomalous encapsulation* observed by Khomami and Ranjbaran (1997). When two polymer melts are coextruded in three layers (A-B-A) through a slit die, with the middle layer being less viscous, the more viscous component encapsulates the less viscous one if the latter is sufficiently thin. The authors suggested that this counter-intuitive phenomenon might be due to the elastic effects, but offered no detailed explanation.

This paper seeks a better understanding of these two phenomena through a thorough computational study of elastic encapsulation in bicomponent stratified flows of viscoelastic fluids. We use an accurate and efficient numerical algorithm, based on a phase-field model, to explore the coupling between interfacial motion and viscoelastic stresses. Our results show that the elastic effect can indeed produce the curtate cycloid shape in a circular pipe, and also cause anomalous encapsulation if the middle layer is thin enough.

## II. THEORETICAL MODEL AND NUMERICAL METHOD

We consider the stratified flow of two viscoelastic fluids in a conduit of arbitrary cross section, schematically shown in Fig. 1. The encapsulation of one component by the other is reflected by the axial evolution of the interface (i.e., along the primary flow direction  $z$ ). The numerical simulation of this process faces at least three challenges: Tracking the interfacial motion, including the moving contact lines on the solid walls; incorporating nonlinear viscoelastic rheology for both components; and the three-dimensionality (3D) of the geometry.

We meet the first two difficulties with a diffuse-interface method recently developed for computing interfacial flows of complex fluids [Yue *et al.* (2004); Feng *et al.* (2005); Yue *et al.* (2006b)]. The theoretical model and numerical algorithm have been detailed before, as are numerical experiments that validate both. Here we only briefly outline the key ideas, list the governing equations, and mention the salient features of the numerical scheme. Take a system of two immiscible Giesekus fluids, for example. We introduce a phase-field variable  $\phi$  to describe the thin but *diffuse interface* between the two components;  $\phi$  equals 1 and -1 in the bulk phases of fluid 1 and fluid 2, and changes smoothly across the interfacial layer. The two components assume concentrations  $c_1 = (1 + \phi)/2$

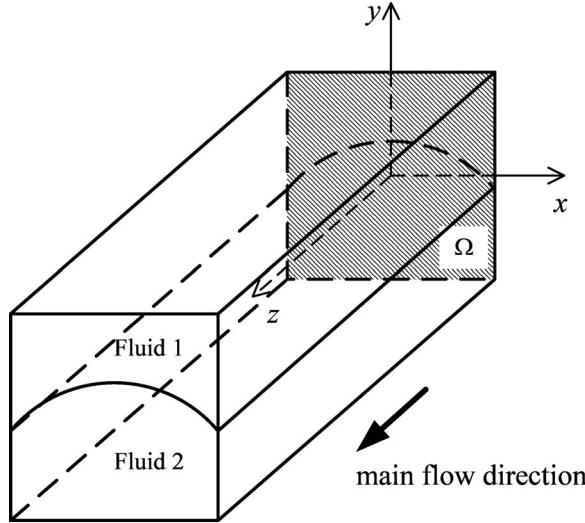


**FIG. 1.** Schematic of the flow channel.

and  $c_2=(1-\phi)/2$ , respectively, and the nominal “interface” is the level set  $\phi=0$ . The governing equations consist of the Cahn–Hilliard equation describing the convection and diffusion of the interface, the linear momentum equation, the continuity equation, and constitutive equations for the viscoelastic fluids:

$$\frac{\partial\phi}{\partial t} + \mathbf{v} \cdot \nabla\phi = \gamma\nabla^2G, \quad (1)$$

$$\rho\left(\frac{\partial\mathbf{v}}{\partial t} + \mathbf{v} \cdot \nabla\mathbf{v}\right) = \nabla \cdot (-p\mathbf{I} + \boldsymbol{\tau}) + G\nabla\phi, \quad (2)$$

$$\nabla \cdot \mathbf{v} = 0, \quad (3)$$

$$\boldsymbol{\tau}_{p,i} + \lambda_{H,i}\boldsymbol{\tau}_{p,i(1)} + \alpha_i \frac{\lambda_{H,i}}{\mu_{p,i}} (\boldsymbol{\tau}_{p,i} \cdot \boldsymbol{\tau}_{p,i}) = \mu_{p,i} [\nabla\mathbf{v} + (\nabla\mathbf{v})^T], \quad (i=1,2), \quad (4)$$

where

$$G = \lambda \left[ -\nabla^2\phi + \frac{\phi(\phi^2 - 1)}{\epsilon^2} \right] \quad (5)$$

is the chemical potential,  $\gamma$  is the Cahn–Hilliard mobility parameter,  $\epsilon$  is the capillary width which is around 1/5 of the interfacial thickness, and  $\lambda$  is the mixing energy that determines the interfacial tension [Yue *et al.* (2004)]:  $\sigma=(2\sqrt{2}/3)(\lambda/\epsilon)$ . The density  $\rho$  is the average between the two components  $\rho=c_1\rho_1+c_2\rho_2$ . The total stress tensor is defined as

$$\boldsymbol{\tau} = \sum_{i=1}^2 c_i [\mu_{s,i} ([\nabla\mathbf{v} + (\nabla\mathbf{v})^T]) + \boldsymbol{\tau}_{p,i}]. \quad (6)$$

Within each component,  $\mu_{s,i}$ ,  $\mu_{p,i}$ ,  $\boldsymbol{\tau}_{p,i}$ ,  $\lambda_{H,i}$ , and  $\alpha_i$  are the solvent viscosity, polymer viscosity, polymer stress, polymer relaxation time, and mobility parameter in the

Giesekus model, where subscript  $i$  denotes the  $i$ th component. The subscript (1) denotes the upper convected derivative. The Oldroyd-B model is recovered when  $\alpha_i=0$ . The Giesekus model is generally appealing because it is molecularly based [Giesekus (1982)] and strikes a balance between simplicity and realistic predictions [Tirtaatmadja and Sridhar (1995)]. In our context, in particular, it is perhaps the simplest nonlinear viscoelastic model to give a meaningful  $N_2$  [Bird *et al.* (1987)].

Several groups have undertaken 3D calculations on the encapsulation in generalized Newtonian fluids [Karagiannis *et al.* (1990); Torres *et al.* (1993)] and viscoelastic fluids [Takase *et al.* (1998); Sunwoo *et al.* (2001, 2002)]. But computational limitations are such that the mesh is invariably too coarse—typically with 6 or 7 grid points across the channel—to yield any information on the structure of the secondary flow. We circumvent the difficulty by reducing the spatial dependence to two dimensional (2D). Since encapsulation is a slow process that occurs over an axial distance of typically more than 100D [Everage (1975); Khomami and Ranjbaran (1997); Dooley *et al.* (1998)], a “lubrication approximation” is appropriate that allows one to simplify the problem to quasi-2D. More specifically, we assume that all flow variables (except pressure  $p$ ) vary slowly in the  $z$  direction:  $\partial/\partial z \ll \partial/\partial x, \partial/\partial y$ , and thus neglect the  $\partial/\partial z$  terms in the governing equations. Since the flow is driven by an axial pressure gradient, we write:

$$p(x, y, z) = \hat{p}(x, y) + p_z z, \quad (7)$$

where the pressure gradient  $p_z$  that drives the primary flow is assumed constant in keeping with the lubrication approximation. Then the unknown variables—the velocity field  $\mathbf{v}=(u, v, w)$ , pressure  $\hat{p}$  and the polymer stresses  $\tau_{p,i}$ —are all defined on the cross-sectional  $x$ - $y$  plane, even though the vectors and tensors retain their 3D components. Encapsulation now consists of the evolution of the interface *in time*, rather than along  $z$ , driven by secondary flows in the cross-sectional plane. To specify the magnitude of the primary flow, one may either fix  $p_z$  and allow the flow rate to evolve in time, or fix the total flow rate [Xue *et al.* (1995); Debbaut *et al.* (1997); Tanoue *et al.* (2006)]

$$Q = \int_{\Omega} w d\Omega \quad (8)$$

through the cross section  $\Omega$  (Fig. 1). The results to be presented are based on the second method, although the first has been implemented in our computations as well. In the finite-element scheme, Eqs. (1)–(8) are solved in a fully coupled manner, and  $p_z$  plays a role similar to a Lagrange multiplier in enforcing the constraint of Eq. (8).

Such quasi-2D models have been used successfully by several groups to predict the secondary flow in single-component pipe flows of viscoelastic fluids [Xue *et al.* (1995); Debbaut *et al.* (1997); Tanoue *et al.* (2006)]. The theoretical and numerical simplification comes at a price, however. The neglect of  $z$  dependence and the assumption of a constant  $p_z$  render the model incapable of predicting *purely viscous encapsulation* in stratified Newtonian fluids. This is because after the lubrication approximation, the viscosity stratification affects only the primary flow  $w$ , and the  $x$  and  $y$  components of Eqs. (2) and (3) become independent of  $w$ . Thus, for Newtonian and generalized Newtonian fluids, the viscosity difference will not produce  $u$  and  $v$  components that would change the interface shape, and the quasi-2D model is unable to predict encapsulation due to viscosity disparity. With this caveat, we limit our attention to *elastically driven* secondary flows.

The governing equations, Eqs. (1)–(5), (8), are solved by a finite-element package AMPHI (Adaptive Meshing for Phase Field  $\phi$ ) that uses adaptive meshing to resolve the narrow interface [Yue *et al.* (2006b)]. P2 elements are used for  $\mathbf{v}$  and  $\phi$ , and P1 elements

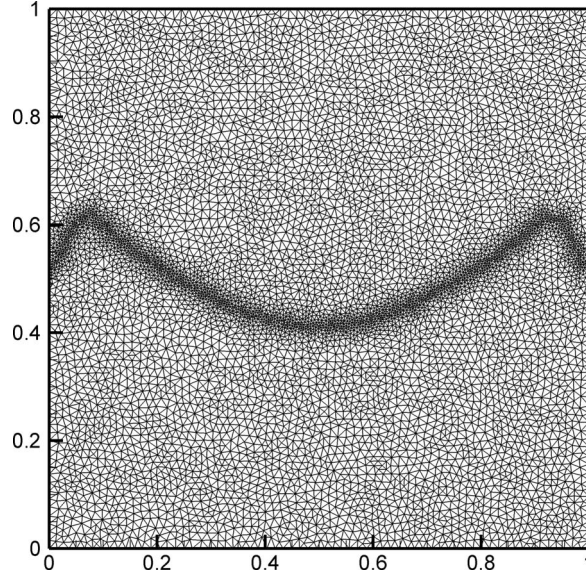


**FIG. 2.** An example of the computational mesh in a square domain of  $1 \times 1$ .

for  $\hat{p}$  and  $\tau_{p,i}$ . Second-order implicit schemes are used for temporal discretization. A general-purpose mesh generator GRUMMP [Freitag and Ollivier-Gooch (1997)] is adopted for the adaptive meshing, and  $\phi$  is used as the criterion of mesh refinement. Figure 2 shows an example of the mesh, with the densest grids deployed in the interfacial region. At the beginning of the simulation, the interface is specified by an initial  $\phi$  field. The numerical toolkit has been validated [Yue *et al.* (2006b)] and proved to be accurate and efficient in simulating many interfacial flows in viscoelastic and nematic fluids [Yue *et al.* (2006a); Zhou *et al.* (2006, 2007), e.g.]. Compared with the AMPHI used in those studies, the current work entails adding the  $z$  components of the unknowns and allowing both fluid components to be viscoelastic. For Newtonian flows through rectangular pipes, the code gives highly accurate results even on a coarse mesh of grid size  $0.1D$ . In the simulations to be presented, we have used a bulk grid size of  $h_0=0.02D$  and interfacial grid size of  $h_1=0.003D$ . Numerical experimentation shows these to be more than sufficient for convergence with respect to grid size. The time step is constrained by interfacial motion such that the interface moves no more than  $h_1$  in one step [Yue *et al.* (2006b)].

### III. NUMERICAL RESULTS

We simulate the stratified flow of two Giesekus fluids in pipes of circular and noncircular cross sections. All variables and parameters are made dimensionless by using the characteristic size of the cross section  $D$ , the total viscosity of the first component  $\mu_1 = \mu_{s,1} + \mu_{p,1}$ , and the average axial velocity of the primary flow  $W=Q/A$ ,  $A$  being the cross section area. The following dimensionless groups are involved:

$$Ca = \frac{\mu_1 W}{\sigma} \quad (\text{Capillary number})$$

$$Re = \frac{\rho_1 WD}{\mu_1} \quad (\text{Reynolds number})$$

$$De = \frac{\lambda_{H,1}W}{D} = \frac{\lambda_{H,1}Q}{AD} \quad (\text{Deborah number})$$

$$Pe = \frac{WD\epsilon^2}{\gamma\lambda} \quad (\text{Peclet number}) \quad (9)$$

$$\beta_i = \frac{\mu_{s,i}}{\mu_i}, \quad i = 1, 2 \quad (\text{Retardation-relaxation time ratio})$$

$$\mu^* = \frac{\mu_2}{\mu_1} \quad (\text{Viscosity ratio})$$

$$\lambda^* = \frac{\lambda_{H,2}}{\lambda_{H,1}} \quad (\text{Relaxation time ratio})$$

along with the density ratio between the two components, the mobility parameter of the Giesekus fluids  $\alpha_1$  and  $\alpha_2$ , and possible geometric ratios characterizing the cross section  $\Omega$ .

In polymer coextrusion experiments,  $\rho \sim 1 \text{ g/cm}^3$ ,  $\mu \sim 10^4 \text{ poise}$ ,  $W \sim 1 \text{ cm/s}$ ,  $D \sim 1 \text{ cm}$  [Debbaut *et al.* (1997)]. If we assume the interfacial tension to be  $\sigma \sim 10 \text{ dyne/cm}$  [Elemsans *et al.* (1990)], then  $Ca \sim 10^3$  and  $Re \sim 10^{-4}$ . Thus for typical materials and flow conditions in coextrusion, inertia and interfacial tension both have negligible effects. In our simulations, we have set  $Re$  to zero, and used a large but finite  $Ca$ . The density ratio drops out along with inertia. Thanks to the diffuse interface model, contact line motion can be simulated without resorting to *ad hoc* slip models [Jacqmin (2000)]. The wetting condition is prescribed through wall-fluid interaction potentials [Khatavkar *et al.* (2007)]. In this work, we use the simplest case of zero wall potential, which produces neutral wetting with an equilibrium contact angle of  $\pi/2$ .

In the following, we first study the elastic encapsulation between two immiscible Giesekus components in a circular pipe. This suppresses the geometric effect on secondary flows and highlights the effect of elasticity contrast across the interface. Then we will simulate three-layer coextrusion in rectangular pipes of different aspect ratios. Now that both effects are present, the interfacial morphology will depend on the outcome of their competition.

### A. Elastic encapsulation in a circular pipe

Figure 3 shows the schematic of coextrusion in a round pipe of diameter  $D$ . For the diffuse interface, we use  $\epsilon = 5 \times 10^{-3}$ ,  $\lambda = 10^{-7}$ , and  $\gamma = 10^{-1}$  in all calculations, which corresponds to  $Ca = 5.3 \times 10^4$  and  $Pe = 2500$ . The two components are assumed to have the same total viscosity and relaxation time:  $\mu^* = 1$ ,  $\lambda^* = 1$ . All results are at a Deborah number  $De = 1$ . The initial interface bisected the circle into two identical parts. Our focus is on how rheology of the components affects the interfacial shape, and this is examined by varying the parameters of the Giesekus model.

We will study the effect of  $N_2$  contrast on the interfacial morphology. To minimize the effect of viscosity, we set the polymer viscosity to be a small portion of the total viscosity:  $\beta_1 = \beta_2 = 0.9$ . Therefore the shear viscosity of the two components are almost identical and the primary flow is nearly axisymmetric. The elasticity contrast is effected via differing mobility parameters:  $\alpha_1 = 0.5$ ,  $\alpha_2 = 0.1$ . The larger  $\alpha_1$  endows the top fluid with a stronger elasticity:  $[\Psi_2(\dot{\gamma})]_1 < [\Psi_2(\dot{\gamma})]_2 < 0$ . Figure 4 shows contours of the primary flow,

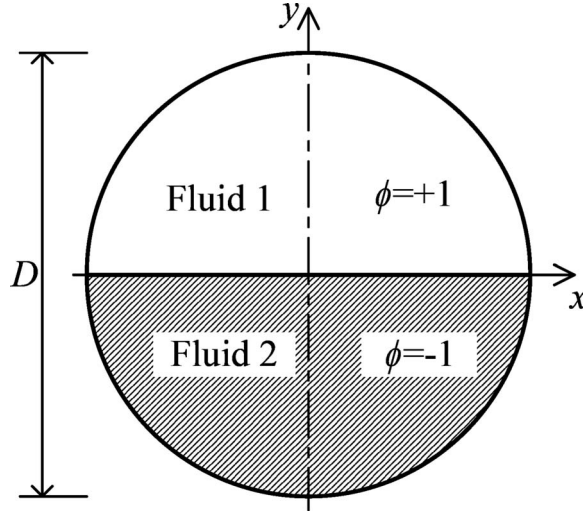


**FIG. 3.** Coextrusion in a circular cross section.

normal stress difference, and secondary flow at  $t=6.79$ . In this relatively early time, the polymer stress has fully developed but the interface has undergone little distortion. The simple kinematics facilitates analysis in the spirit of White *et al.* (1972), who assumed axisymmetric flow and a flat interface.

The distribution of the axial velocity  $w$  is very close to that of a one-component flow, with nearly concentric circular contours. In a one-component flow, this would imply  $\nabla \dot{\gamma} \times \nabla w \approx 0$  and no secondary flow [Yue *et al.* (2008)]. In the two-component system, however, the jump of normal stresses across the interface does induce a secondary flow. The horizontal interface coincides with the shear gradient direction  $\nabla w$ , and the local gradient direction 2 and neutral direction 3 are illustrated for point B near the wall in Fig. 4(a). Thus,  $\tau_{pxx} - \tau_{pyy}$  approximates  $N_2$  along the interface. Across the interface, although

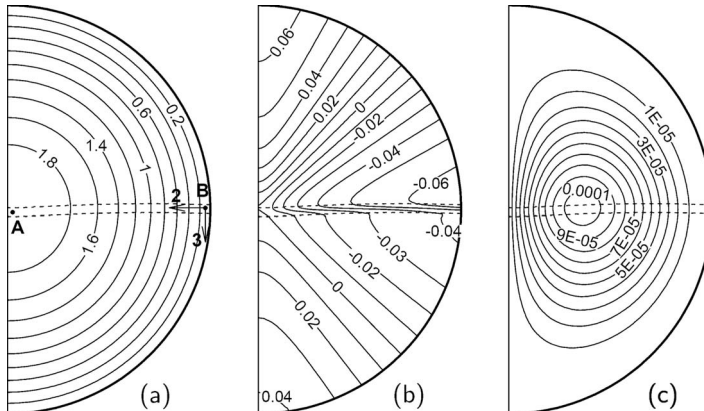


**FIG. 4.** Flow and stress fields in the circular cross section at  $t=6.79$ . Because of symmetry, only the right half of the cross section is shown, and the interface is delineated by the  $\phi = \pm 0.9$  contours (dashed lines). (a) Contours of the axial velocity  $w$ ; (b) contours of the normal stress difference  $\tau_{pxx} - \tau_{pyy}$ ; (c) contours of a stream function  $\psi$  defined by  $\partial\psi/\partial x = -v$  and  $\partial\psi/\partial y = u$ . A positive  $\psi$  indicates counterclockwise secondary flow.  $\alpha_1 = 0.5$ ,  $\alpha_2 = 0.1$ ,  $\beta_1 = \beta_2 = 0.9$ .

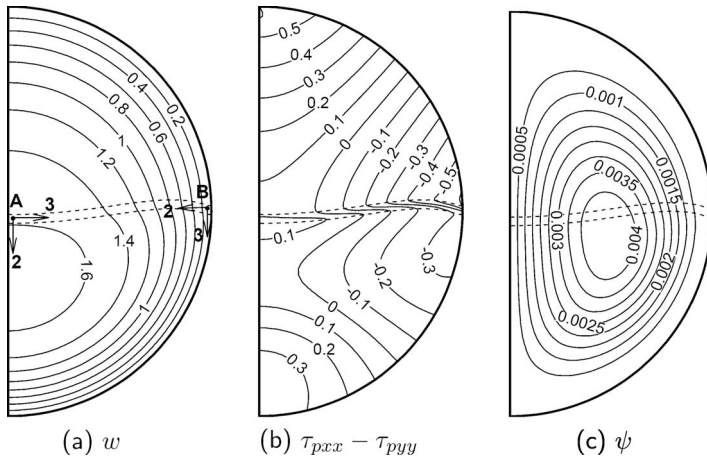


**FIG. 5.** Flow field in the circular cross section at  $t=1.25$ .  $\mu^*=0.5$ ,  $\lambda^*=1$ ,  $\alpha_1=\alpha_2=0.5$ ,  $\beta_1=\beta_2=0.1$ .

$\dot{\gamma}$  is almost constant, the differing  $\Psi_2$  in the two bulk components produces a jump in  $N_2$  across the interface [Fig. 4(b)]. In fact,  $N_2$  would be discontinuous in a sharp-interface representation. From point A to point B along the interface, this jump grows from zero to maximum which is around 0.02. A negative  $N_2$  means that the fluid has an extra compressive stress in the 2 direction or equivalently an extra tensile stress in the 3 direction. Thus the stronger elasticity in the top component produces a stronger upward tensile stress in fluid 1 than the downward stress in fluid 2. This drives an upward flow near the wall and accordingly a downward flow near the center, as is evident in Fig. 4(c). This scenario is consistent with the analysis of White *et al.* (1972). As  $\beta$  is close to unity, the elastic effect is weak in this case and the magnitude of secondary flow  $\sqrt{u^2+v^2}$  is very small with a mean of  $2.8 \times 10^{-4}$  and a maximum of  $1.1 \times 10^{-3}$ .

Real polymer melts and concentrated solutions have much stronger elasticity and shear thinning than represented by  $\beta=0.9$ , and the two components typically have unequal shear viscosities. To reflect this, we reduce the retardation-relaxation time ratio to  $\beta=0.1$  so that the polymer contribution dominates the total viscosity, and set the viscosity ratio to  $\mu^*=0.5$ . If all the other parameters are the same between the two components, fluid 1 will have higher elasticity and viscosity than fluid 2. Figure 5 plots the flow and stress fields as before. Due to different viscosities in the two components, the  $w$  contours deviate visibly from concentric circles. The maximum  $w$  is shifted downward into fluid 2 which has a lower viscosity, as shown in (a). Along the interface, the local gradient direction varies from vertical at point A near the center to horizontal at point B near the wall. Although the flow field is more complex than the previous one, the idea of the more elastic component protruding into the other one still holds. At B, the effect of  $N_2$  stratification is an upward flow as in the previous case. At A, the stronger  $N_2$  in fluid 1 is manifested by a larger downward compressive stress, which further promotes the counterclockwise secondary flow. The streamlines are depicted in Fig. 5(c), with a stronger circulation than in Fig. 4(c). The mean and maximum velocities are  $1.4 \times 10^{-2}$  and  $3.0 \times 10^{-2}$ , respectively. Accordingly, the interfacial motion occurs at a much faster pace than in the previous case.

The interfacial motion continues in time, as the more elastic fluid 1 penetrates downward in the center and the less elastic fluid 2 wraps around along the walls (Fig. 6). Although the fluids obey no-slip boundary conditions on the walls, the three-phase con-

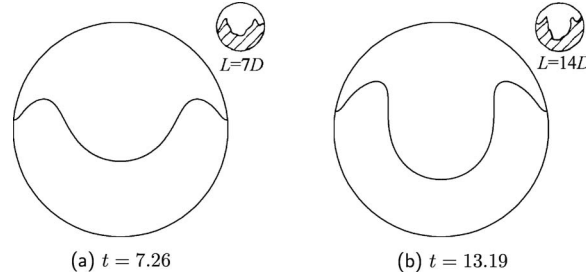


**FIG. 6.** Interface position and stream function at later times.  $\mu^*=0.5$ ,  $\lambda^*=1$ ,  $\alpha_1=\alpha_2=0.5$ ,  $\beta_1=\beta_2=0.1$ . The insets are interface shapes from the coextrusion experiment [Minagawa and White (1975), Fig. 12].  $L$  is the distance from die inlet.

tact line is still subject to motion because of the diffusive dynamics in the Cahn–Hilliard model [Jacqmin (2000)]. This represents an advantage of the diffuse-interface model; a sharp-interface model will have a pinned contact line unless *ad hoc* slip conditions are assigned [White and Lee (1975)]. Because of additional dissipation at the contact line, its upward motion (or the “apparent slip velocity”) lags that of the secondary flow away from the wall. Thus, the interface assumes the shape of a hump near the wall.

As our quasi-2D setup excludes viscous encapsulation, this simulation demonstrates the magnitude of purely elastically driven encapsulation. The average axial velocity being unity, Figs. 6(a) and 6(b) give an indication of the interface shape roughly  $7.26D$  and  $13.19D$  downstream. The interface exhibits the characteristic curtate cycloid shape observed in experiments [Han, 1973; Lee and White (1974); Minagawa and White (1975); Southern and Ballman (1975)]. Furthermore, the computed interfaces at  $t=7.26$  and  $13.19$  closely resemble those experimentally recorded at locations  $L=7D$  and  $14D$  by Minagawa and White (1975). This correspondence is subject to two caveats, however. Because the axial velocity  $w$  varies over the cross section, translating the temporal evolution of the interface into axial evolution is no easy task [Debbaut and Dooley (1999); Anderson *et al.* (2006)]. At a given downstream location, for example, the near-wall part of the interface will have had more time to develop than the central part. So the comparison in Fig. 6 must be viewed in some average sense. Moreover, it is uncertain whether our parameters match the polyethylene melts in the experiment, with and without  $TiO_2$  fillers. No rheological data were given beyond a viscosity ratio. Nevertheless, Fig. 6 provides unequivocal evidence that elasticity stratification can become significant within a distance of roughly  $100D$ , consistent with prior experiment observation [Khomami and Ranjbaran 1997; Debbaut and Dooley (1999); Dooley (2002); Dooley and Rudolph (2003)], and that it is capable of producing the curtate cycloid interface shape in qualitative, and even semiquantitative, agreement with experiments.

It is worthwhile to reexamine the available experimental results, which were previously rationalized by viscous encapsulation, in light of elastic effects. Although Southern and Ballman (1975) did not supply data on the elasticity for the two polystyrene melts (PS-A and PS-B) at  $T=240$  °C, at which the curtate cycloid interface was observed, they did report that PS-B has a larger  $\Psi_1$  than PS-A at  $T=180$  °C. If we take this to mean that PS-B is more elastic at all temperatures, then the observed encapsulation of PS-B by PS-A may be a direct result of elastic encapsulation rather than viscosity crossover. The experiment at  $T=220$  °C, which did not produce a curtate cycloid interface even though the viscosity crossover was present, used a shear rate that is five times smaller than that at 240 °C. The lack of encapsulation may simply be because melt elasticity is not

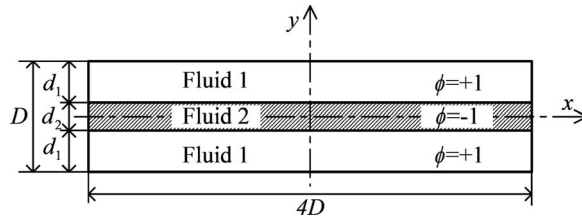


FIG. 7. Three-layer coextrusion in a rectangular cross section.

brought out at such low shear. Similarly [Lee and White \(1974\)](#) observed the curtate cycloid interface in a polymethylmethacrylate (PMMA)/PS system near the viscosity crossover. PS, which has a higher  $|\Psi_2|$  than PMMA, protrudes into PMMA in the center of the tube. This is again consistent with elastic encapsulation as simulated here (Fig. 6). Thus we argue that elastically driven encapsulation is the real reason for the curtate cycloid interface in these experiments. The viscosity crossover probably serves only to minimize the viscosity difference and therefore the effect of viscous encapsulation.

### B. Anomalous encapsulation in a rectangular die

This calculation is motivated by the experiments of [Khomami and Ranjbaran \(1997\)](#) on three-layer coextrusion of two viscoelastic fluids in a rectangular channel, schematically shown in Fig. 7. A high density polyethylene (HDPE) layer is sandwiched between two polypropylene (PP) layers. The HDPE is less viscous and less elastic than the PP, and thus is expected to encapsulate PP according to both viscous and elastic encapsulation. Khomami and Ranjbaran found, however, that this is only true if the HDPE layer is sufficiently thick. When the HDPE layer is below a critical thickness, it becomes entirely enclosed by the PP in an “anomalous encapsulation.” Since the reversal cannot be explained by viscous encapsulation, Khomami and Ranjbaran conjectured that the polymer normal stresses must have played a significant role here. A later publication by the same group [[Khomami and Su \(2000\)](#)] indicates that viscous encapsulation is greatly suppressed if the layer thickness of the less viscous fluid is below a critical value, which also suggests an elastically based mechanism for the anomalous encapsulation. In the following, we will give a clearer explanation through simulation of the elasticity-induced secondary flow.

We consider the three-layer coextrusion of two viscoelastic fluids shown in Fig. 7. Although the rectangular cross section in the experiment has an aspect ratio of 10 [[Khomami and Ranjbaran \(1997\)](#)], an aspect ratio of 4 is found enough to illustrate the physics here and is therefore adopted in the following calculations. The two layers of fluid 1 have a thickness of  $d_1$  and the layer of fluid 2 has a thickness of  $d_2$ . Because of symmetry, we only need to consider the upper right quadrant. The more elastic component (fluid 1) is represented by a Giesekus model, while the less elastic component (fluid 2) is taken to be Newtonian for simplicity. The zero-shear viscosity of the Giesekus component matches the viscosity of the Newtonian component, and we use a large retardation-relaxation time ratio  $\beta_1=0.9$  to minimize the effect of shear thinning in fluid 1. Under this setup, the primary flow is little influenced by the viscoelastic rheology of fluid 1, and the axial velocity distribution does not change much when the layer thickness ratio  $d_2/d_1$  is varied. In presenting the results, all parameters and variables are made dimensionless by  $D$ ,  $W$ , and  $\mu_1$  as before. The diffuse-interface parameters and finite element sizes are the same as in the previous subsection.

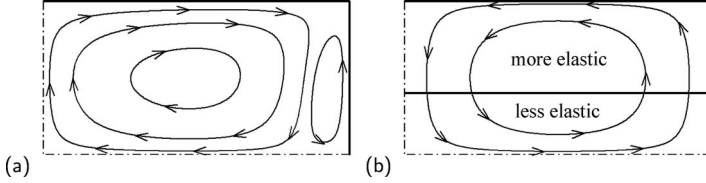


**FIG. 8.** Schematic of secondary flows due to (a) the rectangular cross-sectional geometry; (b) elasticity stratification.

For a single-component viscoelastic fluid flowing in a rectangular duct, the secondary flow consists of two counter-rotating vortices in each quadrant [Yue *et al.* (2008)]. For stratified flows in a circular pipe, elastic stratification produces a secondary flow into the less elastic component in the center of the pipe and into the more elastic one near the wall [cf. Fig. 4(c)]. These two tendencies are both present in the current setup, as schematically depicted in Fig. 8. Thus the secondary flow and encapsulation depend on the competition between the geometric effect and effect of elastic stratification. We explore this competition in a series of computations with varying  $d_2/d_1$ .

The secondary flow of pure fluid 1 is given in Fig. 9(a). The counter-rotating eddies, as explained by Yue *et al.* (2008), are driven by tractions in the cross-sectional plane due to the polymer normal stresses, and the sense of rotation depends on the sign of  $\nabla\dot{\gamma} \times \nabla w$ . When  $d_2/d_1$  is increased to 0.5 [Fig. 9(b)], the counterclockwise vortex next to the sidewall grows at the expense of the central vortex. But still the geometric effect has the upper hand; the clockwise eddy in the middle dominates and the center of the interface has an upward velocity. This implies the encapsulation of the Newtonian middle layer by the Giesekus fluid 1 in time [cf. Fig. 10(a)]. The clockwise central vortex weakens further as  $d_2$  increases and nearly disappears at  $d_2/d_1=2.0$ . Now the geometric effect is overwhelmed by elasticity stratification. For  $d_2/d_1=8.0$  [Fig. 9(e)], the cross section only exhibits one counterclockwise eddy similar to Fig. 8(b); the clockwise eddy has dis-

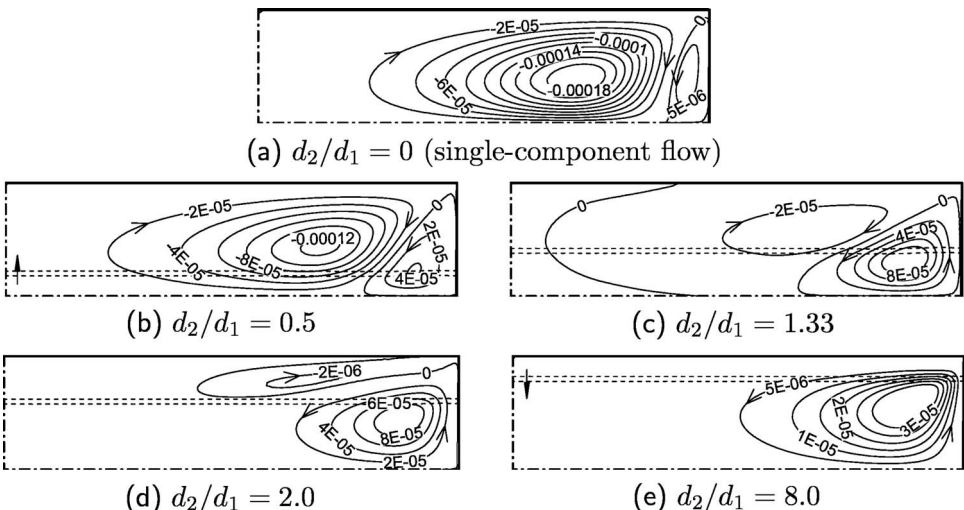


**FIG. 9.** Secondary flow patterns for different layer thicknesses at  $t=6.79$ , depicted by contours of the stream function  $\psi$ . As before, the interface is indicated by dotted lines for the contours  $\phi=\pm 0.9$ .  $De=1$ ,  $\alpha_1=0.5$ ,  $\beta_1=0.9$ ,  $\mu^*=1$ .



**FIG. 10.** Anomalous encapsulation: Comparison of the interfacial shape between our calculation and the experiment. (a) Numerical result at  $t=76.21$  showing the Giesekus fluid (dark) encapsulating the Newtonian fluid (white), with  $De=1$ ,  $\alpha_1=0.5$ ,  $\beta_1=0.1$ ,  $\mu^*=1$ , and initial layer thickness ratio  $d_2/d_1=0.35$ . (b) Experimental picture from [Khomami and Ranjbaran \(1997\)](#) with  $d_2/d_1=0.35$ . © Springer, used with permission.

peared altogether. The secondary flow is such that the Giesekus layers will be encapsulated by the Newtonian layer, as one would expect from elastic stratification analyzed in the last subsection (cf. Fig. 6).

If we magnify the elastic effects by employing  $\beta=0.1$ , the secondary flow gets stronger. Figure 10(a) gives the interface shape at  $t=76.21$  with the initial layer thickness ratio  $d_2/d_1=0.22$ . The majority of the less elastic fluid 2 is trapped at the center of cross section, with a small amount attached to the sidewalls, thus forming an anomalous encapsulation. The configuration of the core is in qualitative agreement with the experimental observation [Fig. 10(b)]. The experimental picture only shows the central region away from the sidewalls, so it is not clear whether a blob of HDPE adheres to the sidewalls as predicted.

Based on the above, we propose that the “anomalous” encapsulation—that of the less elastic HDPE by the more elastic PP for sufficiently thin layers of HDPE—is due to the domination of geometric effect as in a one-phase viscoelastic fluid [[Yue et al. \(2008\)](#)]. In the experiment, the reversal of encapsulation occurs at  $d_2/d_1 \sim 0.4$ . In our simulations, if we use the direction of interfacial motion in the center as the criterion for normal or anomalous encapsulation, the critical thickness is in the range  $d_2/d_1=1.33-2.0$ , thicker than the experimental value. This is probably due to our neglecting viscous encapsulation, which in the experiment should act against the geometric effect. Owing to the lack of  $N_2$  data in the experiment and the absence of viscous encapsulation in our simulation, it is difficult to make more quantitative comparisons.

#### IV. CONCLUSION

We have conducted numerical simulations on interfacial motion in stratified pipe flows of viscoelastic fluids, with the goal of understanding the elastically driven encapsulation of one component by the other. Results show that elastic encapsulation arises through two mechanisms: One due to the mismatch in the second normal stress difference  $N_2$  between the two layers (“elastic stratification”), and the other due to noncircular cross-sectional geometry. These are explained in more specific terms in the following:

1. In a stratified flow of two viscoelastic fluids with negative  $N_2$ , the more elastic component protrudes into the other at the center of the duct while being wrapped by the latter along the sides. In a circular cross section, the interface exhibits a curtate cycloid shape as has been observed experimentally.
2. For bicomponent flows in noncircular ducts, the geometric effect and elasticity stratification may induce interfacial motion in opposite directions, and the outcome of their competition determines the interfacial evolution. In particular, in three-layer coextrusion in a rectangular cross section, normal encapsulation (more elastic com-

ponent wrapped by the less elastic one) gives way to anomalous encapsulation as the middle layer becomes sufficiently thin. This is consistent with prior observations.

We must emphasize that the quasi-2D simplifications used here put two caveats on the results: Viscous encapsulation has been excluded and its interaction with elastic encapsulation cannot be explored; and the interpretation of temporal evolution of the interface as spatial evolution down the pipe is liable to complications [Debbaut and Dooley (1999); Anderson *et al.* (2006)]. These will be remedied in fully 3D computations that are underway. Furthermore, we have left unexplored several factors that are important to the design and optimization of actual extrusion processes, including the composition of the polymer components and more complex cross-sectional geometry of the die [Dooley *et al.* (1998)]. Nevertheless, the current results are not only interesting as a fundamental contribution to non-Newtonian fluid dynamics, but may also benefit polymer processing operations.

## ACKNOWLEDGMENTS

This work was supported by the NSERC, the Canada Research Chair program, the Canada Foundation for Innovation, and the NSFC (Grant Nos. 50390095 and 20674051). C.Z. acknowledges partial support by a University Graduate Fellowship from UBC.

## References

- Anderson, P. D., J. Dooley, and E. H. Meijer, "Viscoelastic effects in multilayer polymer extrusion," *Appl. Rheol.* **16**, 198–205 (2006).
- Bird, R. B., R. C. Armstrong, and O. Hassager, *Dynamics of Polymeric Liquids, Vol. 1. Fluid Mechanics* (Wiley, New York, 1987).
- Debbaut, B., T. Avalosse, J. Dooley, and K. Hughes, "On the development of secondary motions in straight channels induced by the second normal stress difference: Experiments and simulations," *J. Non-Newtonian Fluid Mech.* **69**, 255–271 (1997).
- Debbaut, B., and J. Dooley, "Secondary motions in straight and tapered channels: Experiments and three-dimensional finite element simulation with a multimode differential viscoelastic model," *J. Rheol.* **43**(6), 1525–1545 (1999).
- Dooley, J., "Viscoelastic flow effects in multi-layer polymer coextrusion," Ph.D. thesis, Eindhoven University of Technology, Eindhoven, the Netherlands (2002).
- Dooley, J., K. S. Hyun, and K. Hughes, "An experimental study on the effect of polymer viscoelasticity on layer rearrangement in coextruded structures," *Polym. Eng. Sci.* **38**(7), 1060–1071 (1998).
- Dooley, J., and L. Rudolph, "Viscous and elastic effects in polymer coextrusion," *J. Plast. Film Sheeting* **19**(2), 111–122 (2003).
- Elemans, P. H. M., J. M. H. Janssen, and H. E. H. Meijer, "The measurement of interfacial tension in polymer/polymer systems: The breaking thread method," *J. Rheol.* **34**, 1311–1325 (1990).
- Everage, A. E., "Theory of stratified bicomponent flow of polymer melts. I. Equilibrium Newtonian tube flow," *Trans. Soc. Rheol.* **17**(4), 626–646 (1973).
- Everage, A. E., "Theory of stratified bicomponent flow of polymer melts. II. Interface motion in transient flow," *Trans. Soc. Rheol.* **19**(4), 509–522 (1975).
- Feng, J. J., C. Liu, J. Shen, and P. Yue, "An energetic variational formulation with phase field methods for interfacial dynamics of complex fluids: Advantages and challenges," in *Modeling of Soft Matter*, IMA Volumes in Mathematics and its Applications, edited by M.-C. T. Calderer and E. Terentjev (Springer, New York, 2005), pp. 1–26.
- Freitag, L. A., and C. Ollivier-Gooch, "Tetrahedral mesh improvement using swapping and smoothing," *Int. J.*

- Numer. Methods Eng. **40**, 3979–4002 (1997).
- Giesekus, H., “A simple constitutive equation for polymeric fluids based on the concept of configuration-dependent tensorial mobility,” J. Non-Newtonian Fluid Mech. **11**, 69–109 (1982).
- Han, C. D., “A study of bicomponent coextrusion of molten polymers,” J. Appl. Polym. Sci. **17**, 1289–1303 (1973).
- Han, C. D., *Multiphase Flow in Polymer Processing* (Academic, New York, 1981).
- Jacqmin, D., “Contact-line dynamics of a diffuse fluid interface,” J. Fluid Mech. **402**, 57–88 (2000).
- Joseph, D. D., “Lubricated pipelining,” Powder Technol. **94**, 211–215 (1997).
- Joseph, D. D., and Y. Y. Renardy, *Fundamentals of Two-Fluid Dynamics. Part II: Lubricated Transport, Drops and Miscible Liquids* (Springer-Verlag, New York, 1993).
- Karagiannis, A., A. N. Hrymak, and J. Vlachopoulos, “Three-dimensional studies on bicomponent extrusion,” Rheol. Acta **29**, 71–87 (1990).
- Khan, A. A., and C. D. Han, “On the interface deformation in the stratified two-phase flow of viscoelastic fluids,” Trans. Soc. Rheol. **20**(4), 595–621 (1976).
- Khatavkar, V. V., P. D. Anderson, and H. E. H. Meijer, “Capillary spreading of a droplet in the partially wetting regime using a diffuse-interface model,” J. Fluid Mech. **572**, 367–387 (2007).
- Khomami, B., and M. M. Ranjbaran, “Experimental studies of interfacial instabilities in multilayer pressure-driven flow of polymeric melts,” Rheol. Acta **36**, 345–366 (1997).
- Khomami, B., and K. C. Su, “An experimental/theoretical investigation of interfacial instabilities in superposed pressure-driven channel flow of Newtonian and well characterized viscoelastic fluids. Part I: linear stability and encapsulation effects,” J. Non-Newtonian Fluid Mech. **91**, 59–84 (2000).
- Lee, B. L., and J. L. White, “An experimental study of rheological properties of polymer melts in laminar shear flow and of interface deformation and its mechanisms in two-phase stratified flow,” Trans. Soc. Rheol. **18**(3), 467–492 (1974).
- MacLean, D. L., “A theoretical analysis of bicomponent flow and the problem of interface shape,” Trans. Soc. Rheol. **17**(3), 385–399 (1973).
- Minagawa, N., and J. L. White, “Co-extrusion of unfilled and TiO<sub>2</sub>-filled polyethylene: Influence of viscosity and die cross-section on interface shape,” Polym. Eng. Sci. **15**, 825–830 (1975).
- Southern, J. H., and R. L. Ballman, “Additional observations on stratified bicomponent flow of polymer melts in a tube,” J. Polym. Sci., Polym. Phys. Ed. **13**, 863–869 (1975).
- Sunwoo, K. B., S. J. Park, S. J. Lee, K. H. Ahn, and S. J. Lee, “Numerical simulation of three-dimensional viscoelastic flow using the open boundary condition method in coextrusion process,” J. Non-Newtonian Fluid Mech. **99**, 125–144 (2001).
- Sunwoo, K. B., S. J. Park, S. J. Lee, and K. H. Ahn, “Three-dimensional viscoelastic simulation of coextrusion process: Comparison with experimental data,” Rheol. Acta **41**, 144–153 (2002).
- Takase, M., S. Kihara, and K. Funatsu, “Three-dimensional viscoelastic numerical analysis of the encapsulation phenomena in coextrusion,” Rheol. Acta **37**, 624–634 (1998).
- Tanoue, S., T. Naganawa, and Y. Iemoto, “Quasi-three-dimensional simulation of viscoelastic flow through a straight channel with a square cross section,” J. Soc. Rheol., Jpn. **34**(2), 105–113 (2006).
- Tirtaatmadja, V., and T. Sridhar, “Comparison of constitutive equations for polymer solutions in uniaxial extension,” J. Rheol. **39**, 1133–1160 (1995).
- Torres, A., A. N. Hrymak, J. Vlachopoulos, J. Dooley, and B. T. Hilton, “Boundary conditions for contact lines in coextrusion flows,” Rheol. Acta **32**, 513–525 (1993).
- White, J. L., and B.-L. Lee, “Theory of interface distortion in stratified two-phase flow,” Trans. Soc. Rheol. **19**(3), 457–479 (1975).
- White, J. L., R. C. Ufford, K. R. Dharod, and R. L. Price, “Experimental and theoretical study of the extrusion of two-phase molten polymer systems,” J. Appl. Polym. Sci. **16**, 1313–1330 (1972).
- Wilson, G. M., and B. Khomami, “An experimental investigation of interfacial instabilities in multilayer flow of viscoelastic fluids. II. Elastic and nonlinear effects in incompatible polymer systems,” J. Rheol. **37**(2), 315–339 (1993).
- Xue, S.-C., N. Phan-Thien, and R. I. Tanner, “Numerical study of secondary flows of viscoelastic fluid in straight pipes by an implicit finite volume method,” J. Non-Newtonian Fluid Mech. **59**, 191–213 (1995).

- Yue, P., J. Dooley, and J. J. Feng, "A general criterion for viscoelastic secondary flow in pipes of noncircular cross section," *J. Rheol.* **52**, 315–332 (2008).
- Yue, P., J. J. Feng, C. Liu, and J. Shen, "A diffuse-interface method for simulating two-phase flows of complex fluids," *J. Fluid Mech.* **515**, 293–317 (2004).
- Yue, P., C. Zhou, and J. J. Feng, "A computational study of the coalescence between a drop and an interface in Newtonian and viscoelastic fluids," *Phys. Fluids* **18**, 102102 (2006a).
- Yue, P., C. Zhou, J. J. Feng, C. F. Ollivier-Gooch, and H. H. Hu, "Phase-field simulations of interfacial dynamics in viscoelastic fluids using finite elements with adaptive meshing," *J. Comput. Phys.* **219**, 47–67 (2006b).
- Zhou, C., P. Yue, and J. J. Feng, "Formation of simple and compound drops in microfluidic devices," *Phys. Fluids* **18**, 092105 (2006).
- Zhou, C., P. Yue, and J. J. Feng, "The rise of Newtonian drops in a nematic liquid crystal," *J. Fluid Mech.* **593**, 385–404 (2007).